Contrib Mineral Petrol (1998) 130: 390–396

Craig S. Schwandt · Randall T. Cygan · Henry R. Westrich

Magnesium self-diffusion in orthoenstatite

Received: 22 January 1997 / Accepted: 2 October 1997

Abstract Magnesium self-diffusion coefficients were determined experimentally for diffusion parallel to each of the three crystallographic directions in natural orthoenstatite ($En_{88}Fs_{12}$). Experiments were conducted at 1 atm in CO-CO_2 gas mixing furnaces, which provided oxygen fugacities equivalent to the iron-wüstite buffer. Diffusion of ^{25}Mg was induced in polished samples of oriented orthoenstatite using a film of isotopically enriched ^{25}MgO as the source material. Very short (< 0.15 μm) diffusional penetration profiles were measured by ion microprobe depth profiling. The diffusion coefficients determined for four temperatures (900, 850, 800, 750 °C) provide the activation energies, E_a, and frequency factors, D_o, where $D = D_o \exp(-E_a/RT)$ for Mg self-diffusion parallel to each crystallographic direction: *a*-axis, $E_a = 360 \pm 52$ kJ/mole and $D_o = 1.10 \times 10^{-4}$ m^2/s; *b*-axis, $E_a = 339 \pm 77$ kJ/mole and $D_o = 6.93 \times 10^{-6}$ m^2/s and *c*-axis, $E_a = 265 \pm 66$ kJ/mole and $D_o = 4.34 \times 10^{-9}$ m^2/s. In this temperature range, any possible anisotropy of cation diffusion is very small, however the activation energy for diffusion parallel to the *c*-axis (001) is the lowest and the activation energies for diffusion parallel to the *a*-axis (100) and *b*-axis (010) are higher. Application of these diffusion results to the silicate phases of the Lowicz mesosiderite meteorite provides cooling rates for the silicate portion of the meteorite (4–11 °C/100 years) that are similar, although slower, to previous estimates. These silicate cooling rates are still several orders of magnitude faster than the cooling rates (0.1 °C/10^6 years) for the metal portions.

C.S. Schwandt (✉)
NASA, Johnson Space Center, SN4, Houston,
Tx, 77058-3696, USA
Tel: (281)483-1368; e-mail: cschwand@ems.jsc.nasa.gov

R.T. Cygan · H.R. Westrich
Geochemistry Department, Sandia National Laboratories,
Albuquerque, NM, 87185-0750, USA

Editorial responsibility: T.L. Grove

Introduction

Prior to this investigation, experimentally determined cation diffusion data for orthorhombic pyroxenes did not exist and kinetic modeling, including cooling-rate determinations, was subject to significant uncertainty. Kinetic information for orthopyroxenes has been restricted to theoretical comparison with, and analogy to, a limited number of monoclinic pyroxene diffusion experiments (McCallister and Brady 1979; McCallister et al. 1979; Sneeringer et al. 1984; Fujino et al. 1990), experimental homogenization of exsolution lamellae (Brady and McCallister 1983; Miyamoto and Takeda 1994) and recent theoretical predictions based on Mg - Fe^{2+} order-disorder rate measurements for orthopyroxene (Ganguly and Tazzoli 1993, 1994; Ganguly et al. 1994). Interpreting the petrogenetic histories of terrestrial and meteorite rock systems that involve ortho- and clinopyroxenes requires accurate diffusion information for each mineral type (e.g., Delaney et al. 1981; Lasaga 1983; Smith and Barron 1991). Therefore, magnesium self-diffusion experiments for orthopyroxene were undertaken to provide part of this critical information and to improve our understanding of cation diffusion in silicate minerals.

Magnesium-rich calcium-poor orthopyroxenes have crystal structures that belong to the space group *Pbca* (e.g., Cameron and Papike 1981). Therefore, a complete description of diffusion in these orthorhombic minerals requires the measurement of diffusion along a minimum of three directions within a crystal (Nye 1957). The three orthogonal crystallographic directions *a*, *b*, and *c* were chosen because the crystallographic axes are easily identified in crystals using a petrographic microscope and correspond to the principal axes of diffusion in the crystal; the diffusional fluxes are proportional to the concentration gradients in these respective directions.

Anisotropic diffusion may occur because the ionic site pathways in the orthoenstatite crystal structure are crystallographically distinct. The ordering of cations

between the M1 and M2 sites may also contribute to anisotropy; however in low calcium orthopyroxenes the M1 and M2 sites are similar in size and show much less preference for the ordering of Mg and Fe^{2+} than in clinopyroxenes (Cameron and Papike 1981). Therefore, any directional dependence that binary Mg-Fe^{2+} diffusion or Mg self-diffusion exhibits depends on the ease of cation-site to cation-site transfer of cations through the crystal structure. Three crystallographically distinct pathways exist: (1) Mg cations diffuse along the chains of M1 and M2 octahedral sites which extend parallel to the *c*-axis; (2) Mg cations diffuse parallel to the *b*-axis in planes of M1 and M2 octahedral sites, which are parallel to the (100) plane; (3) Mg cations diffuse parallel to the *a*-axis, which is perpendicular to the alternating tetrahedral and octahedral layers that parallel the (100) plane (Fig. 1). Using these crystallographic constraints and kinetic information pertaining to the ordering of Mg and Fe^{2+} in pyroxenes, Ganguly and Tazzoli (1993, 1994) predicted that the direction of fastest cation diffusion should be parallel to the *c*-axis, because the M1 and M2 octahedra share edges parallel to the *c*-axis. They predicted that cation diffusion along the *b*-axis should be somewhat slower than along the *c*-axis because, in the (100) plane, the chains of M1-M2 sites that extend parallel to the *c*-axis are spaced apart from each other along the *b*-axis. Cation diffusion should be slowest parallel to the *a*-axis because the Mg and Fe^{2+} cations must diffuse through the tetrahedral layers that alternate with the octahedral layers normal to the *a*-direction (Fig. 1).

The studies of cation diffusion in clinopyroxenes used experimental temperatures above 1000 °C to produce diffusion profiles large enough to measure by wavelength-dispersive X-ray analysis using an electron microprobe. However, this approach is not appropriate for *Pbca* orthopyroxene at high experimental temperatures, because at approximately 985 °C orthoenstatite undergoes a structural inversion to protoenstatite which has the *Pbcn* structure (Boyd and Schairer 1964) or possibly to clinoenstatite with a $P2_1/c$ structure (Cameron and Papike 1980). Recent single crystal X-ray diffraction experiments suggest that the *Pbca* to *Pbcn* transition may not occur until about 1087 °C (Yang and Ghose 1995), however, the concern about high temperature diffusion measurements is still valid. Choosing a conservative approach for this study, the structural inversion concern was avoided by conducting the diffusion experiments at temperatures below either inversion temperature. We utilized a thin film approach (Schwandt et al. 1993) for the creation of the diffusion couples, and analyzed the diffusion profiles with an ion microprobe to measure the very short diffusion penetration distances (≈ 0.1 μm) produced at temperatures lower than 1000 °C.

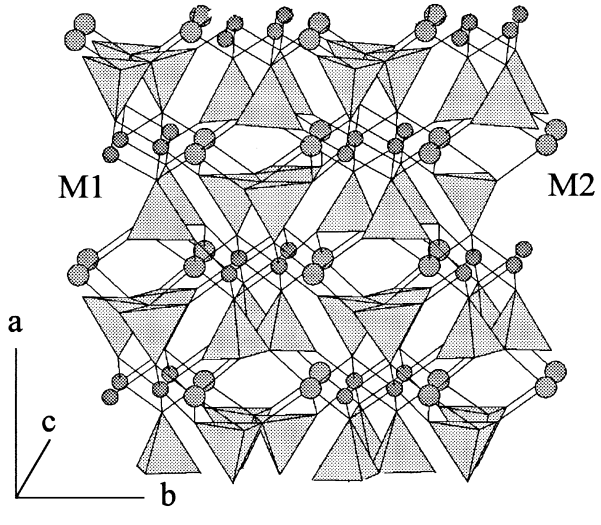

Fig. 1 Crystal model showing partial unit cell for orthoenstatite viewed down the *c*-axis. M1 and M2 chains extend parallel to *c*, but are spaced apart along the *b* direction, and separated by tetrahedral layers in the *a* direction

Experimental approach

Gem-quality orthoenstatite fragments (5 × 10 × 15 mm) from India (exact locality unknown) that are free of inclusions and cleavage fractures were purchased for the matrix of diffusion experiments. Although our preliminary experiments used several different fragments, the diffusion experiments reported here used a single fragment that was cut with a diamond wafer saw into 12 pieces: four pieces oriented normal to each of the three orthogonal directions. Cleavage in orthoenstatite parallels the *c*-axis and its expression on the surface of the crystal fragment was used to orient the fragment for cutting perpendicular to the *c*-axis. Although the sliced pieces are more than a millimeter thick, the gem quality crystals produce excellent optical interference figures that were petrographically monitored to assure the plane of the sectioning cuts was parallel to (001). Any pieces that were not truly *c*-normal were corrected by grinding on a lap wheel. After the (001) cuts were complete the (100) and (010) planes were identified using interference figures and pleochroism, then marked and cut. The extent to which the cuts are perpendicular to the respective axes was limited by our ability to discern the alignment using optical interference figures. However, the alignment of the isogyres was easily observed and deviations from axis-normal orientation were corrected as needed, probably to a precision of ± 5 degrees about each of the axes.

After cutting the crystal fragment, the axis-normal wafers were carefully ground first with 600 grit silicon carbide to avoid development of cleavage traces, and then polished with successively finer diamond pastes to 1 μm. The wafers were then inspected and initially analyzed by standardless quantitative energy-dispersive X-ray spectrometry in a scanning electron microscope, and then later analyzed with an electron microprobe using natural silicate phases as standards. The wafers are homogeneous and nearly endmember enstatite in composition (Table 1), although the analyses parallel to the *c* axis suggest slightly higher concentrations of aluminum that are counterbalanced by lower silicon and slightly higher iron. However, no compositional zoning was observed on the *c*-normal wafers. After initial SEM/X-ray analysis, the orthoenstatite wafers were repolished with 1 μm diamond paste followed by a final polish using 0.06 μm colloidal silica. After the final polish, the oriented enstatite wafers were annealed for 24 hours at the temperature and oxygen fugacity conditions expected for the diffusion experiments. The pre-anneal process was intended to equilibrate the point defect structure of the enstatite to the conditions of the diffusion experiments (see Ryerson et al. 1989). There was no optical petrographic evidence of significant line or planar defects before or after the pre-anneal process.

Table 1 Major element composition of orthoenstatite (oxide wt%). Determined by electron microprobe analysis of each crystallographic surface using natural silicate standards

Oxide	(100)		(010)		(001)	
	Mean	SD	Mean	SD	Mean	SD
SiO_2	57.09	0.24	57.27	0.05	56.81	0.11
Al_2O_3	0.60	0.01	0.62	0.01	0.88	0.04
MgO	34.16	0.22	34.28	0.08	33.22	0.15
FeO	7.96	0.02	7.81	0.02	8.85	0.12
CaO	0.22	0.01	0.22	0.01	0.32	0.07
TiO_2	0.00	0.01	0.01	0.00	0.03	0.01
Cr_2O_3	0.04	0.02	0.04	0.02	0.06	0.01
Total	100.08	0.40	100.26	0.12	100.18	0.24
Number of atoms per 6 oxygens						
Si	1.98		1.98		1.98	
Al	0.02		0.03		0.04	
Mg	1.76		1.77		1.72	
Fe	0.23		0.23		0.26	
Ca	0.01		0.01		0.01	
Ti	0.00		0.00		0.00	
Cr	0.00		0.00		0.00	
sum	4.00		4.02		4.01	
Mole fraction of endmember opx						
En	0.88		0.89		0.86	
Fs	0.12		0.11		0.13	
Wo	0.00		0.00		0.01	

The diffusion source material was placed on the orthoenstatite wafers by thermally evaporating an enriched isotope MgO powder ($^{25}Mg/^{total}Mg = 0.945$) onto the polished pre-annealed orthoenstatite surfaces under high vacuum (Schwandt et al. 1993). The high-vacuum evaporation process produces a film of ^{25}MgO, 1000 to 2000 Å thick, which provides the source material for the self-diffusion (tracer-diffusion) process. Self- or tracer-diffusion coefficients for cations are of a similar order of magnitude as effective binary-cation diffusion coefficients, although self-diffusion of cations in their compositional endmember minerals provides endmember limits for cation diffusion (Cygan and Lasaga 1985; Chakraborty and Ganguly 1992). The use of the term "tracer" in this study refers to the technique of using a specific isotope for "tracing" the diffusion of that isotope through the chemically homogeneous enstatite crystal. True tracer-diffusion coefficients would represent the diffusion of a component that is not found in the host phase prior to the experiment.

The diffusion experiments were run at iron-wüstite (IW) oxygen fugacity conditions using CO-CO_2 gas-mixing furnaces at temperatures of 750, 800, 850, and 900 °C and from several hours to 23.4 days (Table 2) in duration. Oxygen fugacity conditions corresponding to Fe/FeO equilibrium were selected to approximate meteoritic conditions and to maintain the iron in the enstatite at the ferrous valence rather than promoting the development of ferric iron with the use of higher oxygen fugacities. Higher oxygen fugacities and the presence of ferric iron have been shown to enhance cation diffusion in olivine (Buening and Buseck 1973; Lasaga 1981).

Table 2 Self-diffusion coefficients for Mg in orthoenstatite ($En_{90}Fs_{10}$) obtained at IW oxygen fugacity conditions

Direction	D (m^2/s)	Anneal time (h)	T (°C)
(100)	$1.40 \pm 0.28 \times 10^{-20}$	48.0	900
(010)	$1.03 \pm 0.21 \times 10^{-20}$	48.0	900
(001)	$6.70 \pm 1.34 \times 10^{-21}$	48.0	900
(100)	$2.05 \pm 0.41 \times 10^{-21}$	124.6	850
(010)	$8.00 \pm 1.60 \times 10^{-22}$	124.6	850
(001)	$3.20 \pm 0.64 \times 10^{-21}$	124.6	850
(100)	$1.81 \pm 0.36 \times 10^{-22}$	224.7	800
(010)	$1.05 \pm 0.21 \times 10^{-22}$	224.7	800
(001)	$2.20 \pm 0.44 \times 10^{-22}$	224.7	800
(100)	$7.46 \pm 1.49 \times 10^{-23}$	561.6	750
(010)	$6.60 \pm 1.32 \times 10^{-23}$	561.6	750
(001)	$1.90 \pm 3.80 \times 10^{-22}$	561.6	750

In our earlier work (Schwandt et al. 1993, 1995), which examined cation diffusion in garnet we learned that the use of thin films on silicate substrates combined with analysis by ion probe produces an artificial time dependence for D whenever the diffusion penetration distance is especially short. Time series experiments with pyrope (Schwandt et al. 1993) demonstrate that the observed time dependence is entirely analytical and results from a combination of factors. The MgO film is initially smooth and continuous when applied, but sinters into small 1 μm diameter islands during the diffusion experiments. This rough surface topography is replicated by the ion probe during the sputtering process, thereby smearing the analytical film – silicate interface; this effect is especially prominent when diffusion penetration distance into the silicate is only a couple hundred angstroms. We determined that diffusion penetration distances of 1000 Å or greater do not exhibit this time dependence.

Having identified 1000 Å as a minimal analytical limit for this experimental approach, and because we expect cation diffusion in pyroxene to be more rapid than in garnet, we did not conduct a series of time independence experiments. It should be noted, that a separate study by Fisler et al. (in press) directly addresses the issue of the time dependence of diffusion in enstatite using the identical experimental procedure. This subsequent study determined ^{25}Mg self-diffusion rates at 900 °C and the IW buffer that are identical (within the 20% uncertainty reported for the thin film technique) for experimental anneal times ranging from one to eight days, and are in agreement with the results of our work. A preliminary experiment was conducted at 900 °C, and the length of the diffusion parallel to the *b*-axis was used to determine approximately the durations required for all later diffusion anneals in order to provide equivalent distances of diffusion penetration. This approach helps ensure that no artificial time dependence is introduced by our use of the thin film and ion microprobe technique. In addition, given the temperature constraints for the stability of the orthorhombic enstatite structure it is imperative that the diffusion experiments be conducted at relatively low experimental temperatures.

Enstatite samples for each of the three crystallographic directions were run simultaneously at each of the experimental temperatures. After each diffusion experiment the diffusion couples were examined with petrographic and scanning electron microscopes. No evidence of enstatite breakdown or other mineral-forming reactions exists in the samples from these diffusion experiments based upon optical and SEM examinations. However, recent transmission electron microscope analysis of ^{25}Mg self-diffusion using the same technique and enstatite source material, Fisler et al. (in press) have demonstrated the presence of a thin (less than 400 Å) reaction layer of forsterite developed between the enstatite and MgO coating. Even so, the forsterite that forms is enriched in ^{25}Mg and because Mg diffusion in forsterite is relatively rapid (at least two orders of magnitude faster) (cf., Buening and Buseck 1973; Chakraborty 1996), the film and forsterite combination are believed to behave as a thick/infinite source in these experiments.

Analysis of diffusion penetration

Diffusional penetration of the ^{25}Mg into the enstatite was measured with a Cameca IMS 4f ion microprobe, using a depth profiling approach. The primary O- beam of the ion microprobe was rastered perpendicular to the oxide film-enstatite interface. The isotopic composition of ablated or sputtered material in the form of ions was monitored as the rastering primary beam proceeded

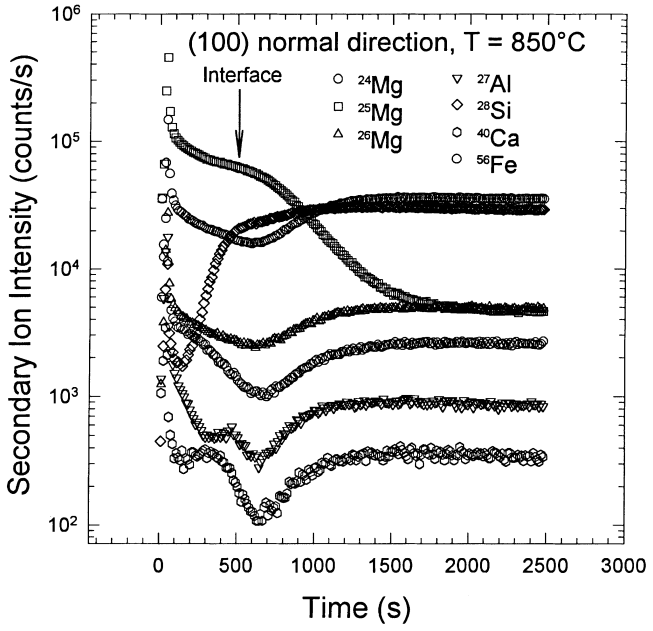

Fig. 2 A typical ion microprobe depth profile analysis with secondary ion intensities plotted versus the analysis time

through the oxide film and into the enstatite crystals. The resulting raw analyses consisted of isotope intensities as a function of analysis time (Fig. 2). The three isotopes of Mg as well as the primary isotopes of Al, Si, Ca, and Fe were acquired for each ion microprobe analysis cycle. The later four elements were included in the analysis to confirm the location of the interface and to identify changes in secondary ionization or the production of any polyatomic species that might have interfered during analysis. The interface between the oxide film and the enstatite is identified in the depth profile by the lack of elements other than Mg in the oxide film, whereas enstatite contains the additional components. Polyatomic interference with the Mg signals is unlikely because there are few possible atomic combinations that could equal 24, 25 or 26 total mass. In addition, the concentration of the Mg isotopes is sufficiently high that any polyatomic interference would be inconsequential, and in fact the proportions of the Mg isotopes in the enstatite past diffusion penetration match the natural proportions of Mg indicating no polyatomic interference. However, as an added precaution, energy filtering techniques were employed to reduce further the possible inclusion of polyatomic species during the analyses (Shimizu and Hart 1982). No changes in secondary ionization were noticed during any of the analyses that might indicate polyatomic interference. The duration of each of the ion microprobe analyses lasted until well after the ^{25}Mg intensity had returned to the natural abundance found in the enstatite (10.0%).

All of the analyses utilized a primary beam acceleration of 10 kV, sample bias offset of 50 V, ± 10 eV window, a 150 μm contrast aperture, a 400 μm field aperture, and a primary beam current of 100 nA. The primary beam was rastered over a 200 × 200 μm area. These parameters provided a linear sputter rate of 1.15 ± 0.05 Å/s. The sputter rate was determined by conducting several depth profile analyses of the enstatite for various durations, and then measuring the depths of the ion microprobe craters with a contact stylus profilometer and dividing the depth by the sputter duration. The several depth measurements yield the same value indicating the sputter rate was constant for the depths of these analyses. In addition, there was no evidence to suggest that secondary ionization was affected by crater depth or side-wall effects. Using the same approach the sputter rate through the MgO film was 1.00 ± 0.05 Å/s. Analysis of an unannealed diffusion couple produced a ^{25}Mg fraction of 0.945 in agreement with the enrichment factor of the ^{25}MgO used for production of the oxide film. This confirms that there was no significant isotope fractionation during production of the oxide film or during the ion microprobe analyses.

Each isotope data set (intensity versus analysis time, e.g., Fig. 2) was converted to a useful format by first determining the exact location within each analysis record that the primary beam penetrated the interface between the oxide film and enstatite (that is, where $x = 0$). During depth profile analysis, secondary ion intensity is enhanced as the primary beam approaches and penetrates an interface between layers, and therefore secondary ion intensity profiles never are step functions (Wilson et al. 1989). A trace amount of aluminum occurs in the orthoenstatite, and as the primary ion beam approaches the oxide film – enstatite interface an inflection occurs in the Mg/Al ratio. We used this inflection of the ratio to help identify the interface. After determination of the position of the interface, the remaining amount of analysis time is converted to distance by multiplying by the sputter rate. Once penetration distance is calibrated, the ratio of ^{25}Mg/^{28}Si is used to determine the diffusion coefficients; monitoring the ^{25}Mg concentration against an element of constant concentration, like ^{28}Si, improves the signal-to-noise and shows the change in ^{25}Mg more clearly than monitoring the ^{25}Mg/total Mg ratio (e.g., Giletti and Casserly 1994). In this way, the decrease in ^{25}Mg intensity due to diffusional penetration is isolated from the complications of changing sensitivity for the magnesium isotopes adjacent to the interface, caused by sputtering through the interface.

Modeling and results

Magnesium self-diffusion coefficients were determined with a diffusion model that provides the best fits to the measured diffusion penetration profiles. The diffusion model should satisfy the initial and boundary conditions that existed during the experiment, such as the ^{25}Mg concentration at the oxide – enstatite interface. Although the oxide film in these experiments is a finite thickness it provides a constant surface concentration of the diffusing isotope (i.e., an infinite source criterion can be applied). The ^{25}Mg/^{28}Si depth profiles are fit with the standard error function equation for Fickian diffusion (Crank 1975):

$$C_x = C_s + (C_b - c_s)\ \mathrm{erf}(x/\sqrt{4Dt}) \quad (1)$$

C_x is the ^{25}Mg/^{28}Si ratio at distance x from the interface, C_b is the initial bulk ratio of the enstatite, and C_s is the ratio in the enstatite at the interface (i.e., $x = 0$). Thus, the C_b term accounts for the amount of naturally abundant ^{25}Mg (relative to ^{28}Si) in the enstatite.

The diffusion coefficient D that provides the best fit to each analysis profile was determined using a nonlinear least squares fitting routine. Uncertainties (1σ) associated with individual curve fit determinations for the Ds of the samples are less than five percent relative. Evaluation of replicate analysis profiles from the preliminary b-axis enstatite experiments indicates that this technique provides Ds with 20 percent relative uncertainties (see Table 2). Therefore the diffusion coefficients are based on a single depth profile analysis and considered to have 20 percent relative uncertainties. Figure 3 compares a typical depth profile with the best model fit to half and twice the model D fit. Diffusion coefficients for each

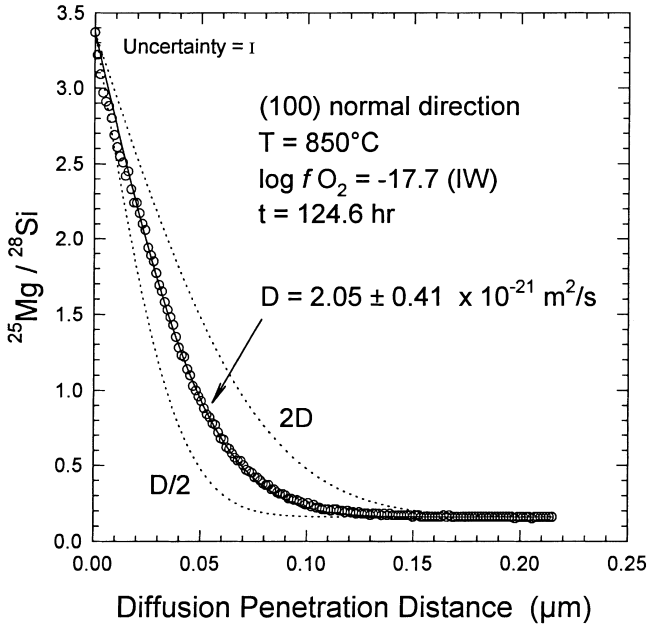

Fig. 3 Measured $^{25}Mg/^{28}Si$ values plotted against diffusion penetration distance are represented by *open circles*. *Solid curve* represents the best fit of the diffusion model to the observed data. *Dashed curves* represent half and twice the best-fit model diffusion coefficient

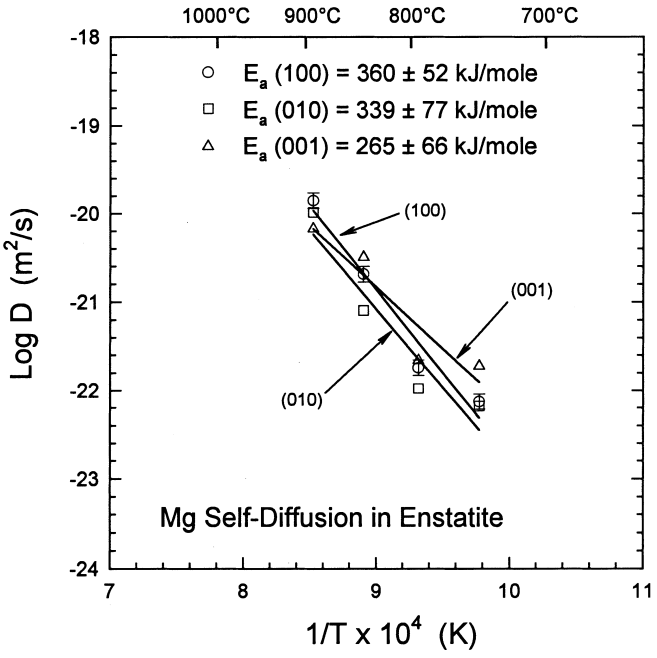

Fig. 4 Arrhenius plot of the experimental ^{25}Mg self-diffusion values for the three crystallographic directions of orthoenstatite obtained at IW oxygen fugacity conditions. The best fit to the measured diffusion coefficients is used to obtain the activation energy for each direction. *Error bars* are only provided for the (100) data for clarity (see text)

experiment are presented in Table 2. Activation energies, E_a, and frequency factors, D_o, based on the Arrhenius relation $D(T) = D_o \exp(-E_a/RT)$, for self-diffusion parallel to each crystallographic direction were derived by linear least squares fitting of the log D values with standard error propagation (see Fig. 4). The resulting Arrhenius values and the corresponding maximum uncertainties (1σ) for each crystallographic direction are presented in Table 3.

Directional anisotropy for the self-diffusion of Mg in the orthopyroxene, if present, is very small for the temperature range of this study; smaller than the 1σ uncertainty for (100) orientation at one temperature (Fig. 4). However, the results suggest that Mg self-diffusion parallel to the *c*-axis may be faster at lower temperatures, except at 900 °C where the values for the three directions are all within 0.35 log units of each other. Although the absolute D values do not display much anisotropy, the resulting activation energies exhibit some differences between the *c*-axis value and those for the *a* and *b* axes. The *c*-axis value of 266 kJ/mole is statistically smaller than the *a*-axis value and may also be unique compared to the *b*-axis activation energy (Table 3). Such that, for the temperature range of 750 to 900 °C, the diffusional anisotropy for Mg, although minor, basically complies with expectation based purely on interpretation of a rigid, charge-balanced structure model, where $D_{(001)} > D_{(010)} > D_{(100)}$.

Log D values for Mg self-diffusion in orthoenstatite are greater than Mg self-diffusion in pyrope garnet, determined using the same technique (Schwandt et al. 1995), but smaller than the values for olivine (Buening and Buseck, 1973; Chakraborty, 1996) (Fig. 5). The log D values for orthoenstatite, especially parallel to the *c*-axis, are similar to the theoretical values determined for orthoferrosilite by Ganguly and Tazzoli (1993, 1994). The differences may reflect the compositional effect of the Fe^{2+} to Mg ratio of the orthopyroxene on the Mg self-diffusion coefficient. The extrapolated Ca diffusion values of Fujino et al. (1990), as referenced by Miyamoto and Takeda (1994) for clinopyroxenes (Fig. 5), are much smaller at 900 °C and are similar to our data at 800 °C and lower temperatures. This may also be indicating a compositional effect on the diffusion of cations through pyroxene. However, caution must be exercised when extrapolating these diffusion values for intercomparison across a wide temperature range due to potential changes in the diffusion mechanisms (Lasaga 1981). Figure 5 demonstrates the range of cation diffusion measurements that have been conducted and highlights how much work yet remains to be done to understand better the effects of composition, oxygen fugacity and pressure.

Table 3 Arrhenius values for orthogonal directions in orthoenstatite ($En_{90}Fs_{10}$) obtained at IW oxygen fugacity conditions

	(100)	(010)	(001)
E_a (kJ/mol)	360 ± 52	339 ± 77	265 ± 66
Log D_o (m^2/s)	−3.96 ± 2.48	−5.16 ± 3.69	−8.36 ± 3.27

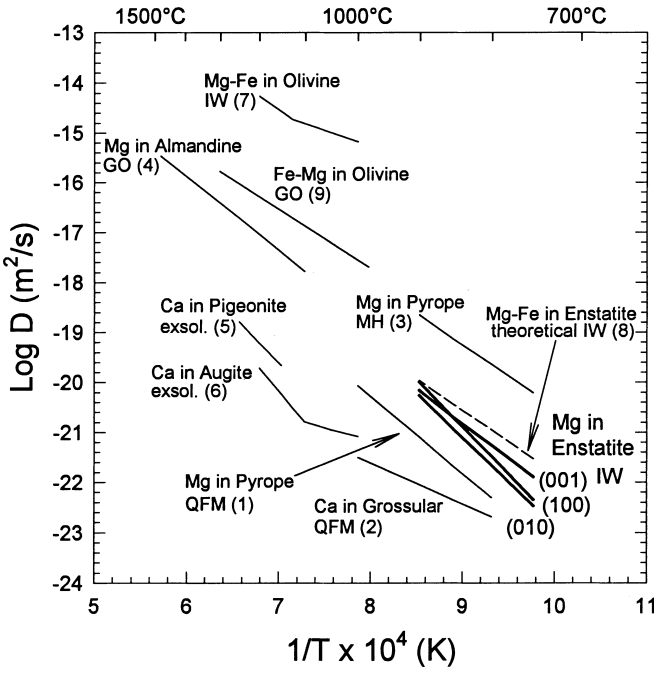

Fig. 5 Arrhenius compilation of cation diffusion values for pyroxene, olivine, and garnet, determined using various techniques (*1* Schwandt et al. 1995, *2* Schwandt et al. 1996, *3* Cygan and Lasaga 1985, *4* Chakraborty and Ganguly 1992, *5* Brady and McCallister 1983, *6* Miyamoto and Takeda 1994, *7* Buening and Buseck 1973, *8* Ganguly and Tazzoli 1994, *9* Chakraborty 1996). No corrections were made for differences in composition, pressure or oxygen fugacity. *Labels* indicate measured cations and minerals used in experiments. Experimental oxygen fugacity conditions are noted when reported in the original study. (solid state buffer assemblages: *GO* graphite-oxygen, *IW* iron-wüstite, *QFM* quartz-fayalite-magnetite, *MH* magnetite-hematite). *Exsol.* denotes diffusion values obtained from homogenization experiments of exsolved lamellae in clinopyroxenes

Applications

When natural minerals contain compositional zoning, there is the potential to extract information about processes occurring during mineral formation and subsequent modification in response to later external conditions. In such cases, accurate cation diffusion coefficients are important parameters for modeling the rate of cooling that occurred during tectonic uplift events (e.g., Lasaga, 1983; Bohlen, 1987; Crowley and Spear, 1987; Medaris et al. 1990; Crowley, 1991; Sharp and Essene, 1991), or estimating the rates of cooling in the parent bodies of meteorites (e.g., Delaney et al. 1981; Ganguly and Tazzoli, 1993; Ganguly et al. 1994; Miyamoto and Takeda, 1994). Selection of appropriate and accurate diffusion coefficients is critical to the resulting interpretation.

The application of diffusion data to meteorites is interesting for cosmological reasons because meteorites provide clues about the formation of the early solar system and planetary bodies. Mesosiderite meteorites are particularly intriguing because they are composed of approximately equal portions of interspersed silicate clasts and Fe-Ni metal. Thus, mesosiderites either represent examples of the metal core – silicate mantle boundary of planetoids, or, alternatively, are the result of impact events on the surface of planetoids (Jones 1982; Hewins 1983; Rubin and Mittlefehldt 1993). Understanding the cooling histories of the metal and the silicate portions of the meteorite would help in choosing critically between the two hypotheses.

The Lowicz meteorite contains exceptionally well preserved zoning between magnesium-rich orthopyroxene ($En_{83}Fs_{17}$) cores and iron-rich orthopyroxene ($En_{63}Fs_{37}$) overgrowths (Delaney et al. 1980). The compositional boundaries between these cores and overgrowths are not sharp but grade between the regions suggesting diffusional re-equilibration during cooling. Delaney et al. (1980, 1981) modeled the cooling rates from a zoning profile in a Lowicz orthopyroxene. Because cation diffusion coefficients for enstatite were not available at that time, Delaney et al. (1980, 1981) estimated, based on the crystal-chemical rationale of Dowty (1980), that the diffusion coefficients for enstatite were similar to those of olivine; they extrapolated the olivine Arrhenius line in Fig. 5 to the lower temperatures of the application. Their modeling effort yielded silicate phase cooling rates in the range of 1 to 100 degrees per day. This flash cooling contrasts with the seemingly unrealistically slow cooling indicated for the metal portion for which a cooling rate of about 0.1 degrees per million years was determined (Powell 1969). These very disparate results would seem to preclude the origin of mesosiderite from the interior of a planetoid. Unfortunately, the calculated cooling rates for the silicate portions of the mesosiderite are based on estimated diffusion coefficients and therefore may be quite inaccurate.

Ganguly et al. (1994) repeated the modeling of the silicate portions of the same mesosiderite meteorites as Delaney et al. (1980, 1981) using the predicted orthopyroxene diffusion coefficients of Ganguly and Tazzoli (1993, 1994) derived from experimental cation order-disorder kinetics. These modeling results indicate that, while the mesosiderite silicates cooled rapidly, it was at a rate of about 1 degree per 100 years, rather than 1 degree per day. Combining the Mg self-diffusion values of the present study with the Ganguly et al. (1994) cooling equations, we obtain a mesosiderite cooling rate of 4 to 11 degrees per 100 years dependent on the diffusional anisotropy. This slightly faster cooling rate is a limiting case because the cooling rate model is based on a binary Mg-Fe^{2+} diffusion coefficient rather than Mg self-diffusion coefficients. Nonetheless, the cooling rate obtained using the experimentally based diffusion coefficients are quite similar to the Ganguly et al. (1994) cooling rate that was derived from theoretically determined diffusion coefficients. A difference of about five orders of magnitude still exists between the cooling rates for the silicate and metal portions; however, the metallographic cooling textures originate at much lower temperatures suggesting that the cooling rates are complementary (Ganguly et al. 1994). Even so, debate as to the origin of mesosiderites continues.

Acknowledgments We are indebted to Graham Layne for his assistance with the University of New Mexico-Sandia National Laboratories ion microprobe facility, and to George Edgerly for his help with the oxide film work. Diana Fisler provided a critical review of an early draft of the paper. We appreciate thorough reviews by Jiba Ganguly and Steve Mackwell. This research was sponsored by the Geosciences Program of the U.S. Department of Energy, Office of Basic Energy Sciences under contract DE-AC04-94AL85000 with Sandia National Laboratories.

References

Bohlen SR (1987) Pressure-temperature-time paths and a tectonic model for the evolution of granulites. J Geol 95: 617–632

Boyd FR, Schairer JF (1964) The system $MgSiO_3$-$CaMgSi_2O_6$. J Petrol 5: 275–309

Brady JB, McCallister RH (1983) Diffusion data for clinopyroxenes from homogenization and self-diffusion experiments. Am Mineral 68: 95–105

Buening DK, Buseck PR (1973) Fe-Mg lattice diffusion in olivine. J Geophys Res 78: 6852–6862

Cameron M, Papike JJ (1980) Crystal chemistry of silicate pyroxenes. In: C.T. Prewitt, (ed) Pyroxenes (Reviews in mineralogy, vol. 7) Mineral Soc Am, pp. 5–92

Cameron M, Papike JJ (1981) Structural and chemical variations in pyroxenes. Am Mineral 66: 1–50

Chakraborty S (1996) Rates and mechanisms of Fe-Mg interdiffusion in olivine at 980–1300 °C. J Geophys Res 102: 12317–12331

Chakraborty S, Ganguly J (1992) Cation diffusion in aluminosilicate garnets: experimental determination in spessartine-almandine diffusion couples, evaluation of effective binary diffusion coefficients, and applications. Contrib Mineral Petrol 111: 74–86

Crank J (1975) The mathematics of diffusion, 2nd edn. Oxford Univ Press, Oxford

Crowley PD (1991) Thermal and kinetic constraints on the tectonic applications of thermobarometry. Mineral Mag 55: 57–69

Crowley PD, Spear FS (1987) The *P-T* evolution of the Middle Köli Nappe Complex, Scandinavian Caledonides (68 N) and its tectonic implications. Contrib Mineral Petrol 95: 512–522

Cygan RT, Lasaga AC (1985) Self-diffusion of magnesium in garnet at 750 to 900 °C. Am J Sci 285: 328–350

Delaney JS, Bedell RL, Harlow GE, Nehru CE, Klimentidis R, Prinz M (1980) Pyroxene overgrowth textures: evidence for rapid cooling from high temperatures in mesosiderites. Lunar Planet Sci Conf XI: 204–206

Delaney JS, Nehru CE, Prinz M, Harlow GE (1981) Metamorphism in mesosiderites. Proc Lunar Planet Sci 12B: 1315–1342

Dowty E (1980) Crystal-chemical factors affecting the mobility of ions in minerals. Am Mineral 65: 174–182

Fisler DK, Cygan RT, Westrich HR (in press) The effects of composition and oxygen fugacity on magnesium self-diffusion in enstatite. Phys Chem Miner

Fujino K, Naohara H, Momoi H (1990) Direct determination of cation diffusion coefficients in pyroxenes. EOS Trans Am Geophys Union 71: 943

Ganguly J, Tazzoli V (1993) Fe^{2+}-Mg interdiffusion in orthopyroxene: constraints from cation ordering and structural data and implications for cooling rates of meteorites. Lunar Planet Sci Conf XXIV: 517–518

Ganguly J, Tazzoli V (1994) Fe^{2+}-Mg interdiffusion in orthopyroxene: Retrieval from the data on intracrystalline exchange reaction. Am Mineral 79: 930–937

Ganguly J, Yang H, Ghose S (1994) Thermal history of mesosiderites: quantitative constraints from compositional zoning and Fe-Mg ordering in orthopyroxenes. Geochim Cosmochim Acta 58: 2711–2723

Giletti BJ, Casserly JED (1994) Strontium diffusion kinetics in plagioclase feldspars. Geochim Cosmochim Acta 58: 3785–3793

Hewins RH (1983) Impact versus internal origins for mesosiderites. In: Proc 14th Lunar Planet Sci Conf, J Geophys Res 88, PP257–B266

Jones JH (1982) Mesosiderites: (1) reevaluation of cooling rates and (2) experimental results bearing on the origin of metal. Lunar Planet Sci Conf 14: 351–352

Lasaga AC (1981) The atomistic basis of kinetics: defects in minerals. In: Lasaga AC, Kirkpatrick RJ (eds) Kinetics of geochemical processes. (Reviews Mineralogy vol.8) Mineral Soc Am, Washington, DC, pp 216–319

Lasaga AC (1983) Geospeedometry: an extension of geothermometry. In: Saxena SK (ed) Kinetics and equilibrium in mineral reactions. Springer-Verlag, Berlin Heidelberg New York, pp 81–114

McCallister RH, Brady JB (1979) Self-diffusion of calcium in diopside (abstract). Geol Soc Am Abstr Program 11: 474

McCallister RH, Brady JB, Mysen BO (1979) Self-diffusion of calcium in diopside. Carnegie Inst Wash Yearb 78: 574–577

Medaris LG Jr, Wang HF, Misar Z, Jelinek E (1990) Thermobarometry, diffusion modelling and cooling rates of crustal garnet peridotites: two examples from the Bohemian Massif. Lithos 25: 189–202

Miyamoto M, Takeda H (1994) Evidence for excavation of deep crustal material of a Vesta-like body from Ca compositional gradients in pyroxene. Earth Planet Sci Lett 122: 343–349

Nye JF (1957) Physical properties of crystals. Clarendon Press, Oxford

Powell BN (1969) Petrology and chemistry of mesosiderites. I. Textures and composition of nickel-iron. Geochim Cosmochim Acta 33: 789–810

Rubin AE, Mittlefehldt DW (1993) Evolutionary history of the mesosiderite asteroid: a chronologic and petrologic synthesis. Icarus 101: 201–212

Ryerson FJ, Durham WB, Cherniak DJ, and Lanford WA (1989) Oxygen diffusion in olivine: effect of oxygen fugacity and implications for creep. J Geophys Res 94, B4: 4105–4118

Schwandt CS, Cygan RT, Westrich HR (1993) A thin film approach for producing diffusion couples. Pure Appl Geophys 103: 631–642

Schwandt CS, Cygan RT, Westrich HR (1995) Mg self-diffusion in pyrope garnet. Am Mineral 80: 483–490

Schwandt CS, Cygan RT, Westrich HR (1996) Calcium self-diffusion in grossular garnet. Am Mineral 81: 448–451

Sharp ZD, Essene EJ (1991) Metamorphic conditions of an Archean core complex, the northern Wind River Range, Wyoming. J Petrol 32: 241–273

Shimizu N, Hart SR (1982) Application of the ion microprobe to geochemistry and cosmochemistry. Ann Rev Earth Planet Sci 10: 483–526

Smith D, Barron BR (1991) Pyroxene-garnet equilibration during cooling in the mantle. Am Mineral 76: 1950–1963

Sneeringer M, Hart SR, Shimizu N (1984) Strontium and samarium diffusion in diopside. Geochim Cosmochim Acta 48: 1589–1608

Wilson RG, Stevie FA, and MaGee CW (1989) Secondary ion mass spectrometry: a practical handbook for depth profiling and bulk impurity analysis. John Wiley and Sons, New York

Yang H, Ghose S (1995) High temperature single crystal X-ray diffraction studies of the ortho-proto phase transition in enstatite, $Mg_2Si_2O_6$ at 1360 K. Phys Chem Miner 22: 300–310